Formulation of local numerical methods in linear elasticity

Article *in* Multidiscipline Modeling in Materials and Structures · June 2020

DOI: 10.1108/MMMS-05-2018-0094

3 authors:

Tiago da Silva Oliveira
Instituto de Educação Superior de Brasília
19 PUBLICATIONS **49** CITATIONS
SEE PROFILE

Wilber Vélez
University of Antioquia
13 PUBLICATIONS **31** CITATIONS
SEE PROFILE

Artur Portela
University of Brasília
58 PUBLICATIONS **1,441** CITATIONS
SEE PROFILE

Formulation of local numerical methods in linear elasticity

Tiago Oliveira, Wilber Vélez and Artur Portela
Department of Civil Engineering, University of Brasilia, Brasilia, Brazil

Received 11 May 2018
Revised 19 June 2018
Accepted 12 September 2018

Abstract

Purpose – This paper is concerned with new formulations of local meshfree and finite element numerical methods, for the solution of two-dimensional problems in linear elasticity.

Design/methodology/approach – In the local domain, assigned to each node of a discretization, the work theorem establishes an energy relationship between a statically admissible stress field and an independent kinematically admissible strain field. This relationship, derived as a weighted residual weak form, is expressed as an integral local form. Based on the independence of the stress and strain fields, this local form of the work theorem is kinematically formulated with a simple rigid-body displacement to be applied by local meshfree and finite element numerical methods. The main feature of this paper is the use of a linearly integrated local form that implements a quite simple algorithm with no further integration required.

Findings – The reduced integration, performed by this linearly integrated formulation, plays a key role in the behavior of local numerical methods, since it implies a reduction of the nodal stiffness which, in turn, leads to an increase of the solution accuracy and, which is most important, presents no instabilities, unlike nodal integration methods without stabilization. As a consequence of using such a convenient linearly integrated local form, the derived meshfree and finite element numerical methods become fast and accurate, which is a feature of paramount importance, as far as computational efficiency of numerical methods is concerned. Three benchmark problems were analyzed with these techniques, in order to assess the accuracy and efficiency of the new integrated local formulations of meshfree and finite element numerical methods. The results obtained in this work are in perfect agreement with those of the available analytical solutions and, furthermore, outperform the computational efficiency of other methods. Thus, the accuracy and efficiency of the local numerical methods presented in this paper make this a very reliable and robust formulation.

Originality/value – Presentation of a new local mesh-free numerical method. The method, linearly integrated along the boundary of the local domain, implements an algorithm with no further integration required. The method is absolutely reliable, with remarkably-accurate results. The method is quite robust, with extremely-fast computations.

Keywords Work theorem, Local weak form, Local mesh-less method, Local meshfree method, Local finite element method, Local formulation

Paper type Research paper

1. Introduction

The main feature of local meshfree and finite element numerical methods is the enforcement of a solution paradigm defined by a node-by-node calculation, to generate the rows of the global system of equations of the body's discretization.

The work theorem has been postulated as a unifying basis in the formulation of numerical methods in continuum mechanics, as early reported by Portela (1981) and Brebbia *et al.* (1985). Recently, the work theorem was applied in the formulation of local meshfree numerical methods, in the set of kinematically admissible strain fields, as reported by Oliveira and Portela (2016). This paper presents a new linearly integrated local form of the work theorem, kinematically formulated, which leads to a point–wise discrete form of equilibrium of tractions, of the local domain associated to each node.

Meshfree numerical methods achieved a remarkable progress over the past few years, see Chen *et al.* (2017), for a recent review. The essential feature of these methods is that they

The first and the second authors acknowledge CNPq – Brazilian National Counsel of Technological and Scientific Development for their scholarships. They also acknowledge the program PECC – Pós-Graduação em Estruturas e Construção Civil, Department of Civil Engineering, University of Brasília.

Multidiscipline Modeling in Materials and Structures

1573-6105
DOI 10.1108/MMMS-05-2018-0094

perform the discretization of the problem domain and boundaries with a set of scattered field nodes that do not require any mesh for the approximation of the field variables.

Smoothed particle hydrodynamics (SPH), presented by Lucy (1977) and Gingold and Monaghan (1977), is one of the earliest meshfree methods applied to solve problems in astrophysics. Libersky *et al.* (1993) were the first to apply SPH in solid mechanics. SPH is based on a strong-form formulation of the weighted residual method, with a Lagrangian description.

The collocation method is also based in the weighted residual strong-form formulation. Typical meshfree collocation methods were published by Kansa (1990); Wu (1992); Zhang *et al.* (2001); Liu *et al.* (2002a); Onate *et al.* (1996); Lee and Yoon (2004) and Jamil and Ng (2013). Collocation methods have some attractive advantages over other meshfree methods, as they implement a simple algorithm, with no integration required. Despite these advantages, collocation methods tend to be inaccurate and unstable, due to the ill-conditioned system of equations.

Other meshfree methods are based on a weighted residual weak-form formulation, which derives the system of algebraic equations through a process of numerical integration using background cells constructed in the problem's domain. The reproducing kernel particle method (RKPM), presented by Liu *et al.* (1995), and the element-free Galerkin (EFG) method, presented by Belytschko *et al.* (1994), were the first weak-form meshfree methods applied in solid mechanics. Melenk and Babuska (1996) presented the partition of unity finite element method (PUFEM). Strouboulis *et al.* (2000) presented the generalized finite element method (GFEM) and pointed out that different partition of unities can be used for the usual approximation and the enrichment.

All these weak-form meshfree methods require the use of a background mesh for integration of the weighted residual weak form over the global problem's domain, and therefore, they are not truly meshfree methods. To overcome this difficulty, a class of meshfree methods based on local weighted residual weak forms, such as the meshfree local Petrov–Galerkin (MLPG) method presented by Atluri and Zhu (1998) to Atluri and Shen (2002), the local point interpolation method (LPIM) presented by Liu and Gu (2001) and the local radial point interpolation method (LRPIM) presented by Liu *et al.* (2002b), have been developed. The main feature of the popular MLPG method is that local weak forms are used for integration on local domains, rather than global weak forms and consequently the method does not require the use of a background global mesh, but only local background cells.

In some particular applications, local meshfree methods exhibit excellent performance. Despite of their performance, local meshfree methods have not succeeded in replacing the standard displacement assumed finite element method (FEM), in general applications.

It is well known that the global formulation of the standard FEM considers a solution paradigm that implements an element-by-element stiffness calculation, which is assembled into the global stiffness matrix. This method of generating the final system of equations is not suitable for the analysis processing in parallel environments. Furthermore, the mesh generation process often becomes a serious bottleneck in large-scale parallel computing, especially when the problem under analysis requires frequent mesh refinement, as in the case, for instance, of moving boundary, crack propagation or large deformation problems. In order to overcome this difficulty, various FEM-based meshfree methods have been proposed, in which finite elements are employed for discretization of the governing equation but are not given explicitly. This is the case of the generalized finite element method GFEM (Melenk, 1995), the partition of unity finite element method PUFEM (Melenk and Babuska, 1996), the manifold method presented by Shi (1991), the voxel finite element method presented by Hollister and Kikuchi (1994), the extended finite element method X-FEM (Belytschko and Black, 1999), the finite cover method presented by Jin and Suzuki (2000) and the overlapping

finite element method presented by Zhang and Bathe (2017) which are denominated as FEM-based meshfree methods.

Therefore, there is still a clear need for an alternative modeling strategy, directly suited for the analysis processing in parallel environments. In order to fulfill this need, this paper presents new local formulations of FEM, which consider a solution paradigm based on a node-by-node calculation, to generate the respective rows of the global system of equations. The non-zero components of the global matrix in the rows of a node correspond to the components derived from the nodes of the local domain of that node. In this case, the analysis processing can easily be parallelized, in terms of nodes, due to the independence of the nodal equations. Nevertheless the final system of equations, obtained by the node-by-node solution paradigm, is equivalent to that obtained by the element-by-element solution paradigm of the standard FEM. Furthermore, in local formulations of FEM, the independence of nodal equations allows using of enrichment of a particular nodal stiffness matrix, in the manner of XFEM, without increasing the nodal degrees of freedom.

A linearly integrated local form that represents a point–wise discrete form of equilibrium of tractions is presented in this paper. The reduced integration performed by this local formulation induces a reduction of the nodal stiffness which, in turn, has the desirable effect of increasing the solution accuracy and, what is most important, presents no instabilities at all, unlike nodal integration methods without stabilization.

The issue of numerical stability is quite significant when developing numerical methods. In the standard FEM, elements with a reduced number of integration points are routinely employed because they are computationally very effective and avoid locking problems of fully integrated elements. As a side effect, such reduced integrated elements are susceptible to spurious singular modes, so-called hourglass modes, which are zero-energy modes in the sense that the element deforms without an associated increase of the elastic energy. These spurious modes, generated by a reduced number of integration points, can be prevented through stabilization techniques. Zienkiewicz and Taylor (1983) and Bathe (2014) provide additional information on this concept.

The reduced integration is the main source of the numerical instability of some meshfree methods, leading to unstable hourglass deformation and zero energy modes. This is the case of the EFG method, see Beissel and Belytschko (1996), and the meshfree particle method, as reported by Belytschko *et al.* (2000). Nodal integration, in meshfree methods without stabilization, leads to instabilities due to the fact that each node is associated with a support domain, where integrations are carried out, to compute the nodal stiffness. This implies that each integration domain is associated with only one integration point, that is the node and hence, when only one integration point is considered for higher order functions, other than constant strain, the nodal integration causes instabilities. In contrast, the new integrated numerical methods presented in this paper consider, in the case of the meshfree method, a total of four integration points to compute the stiffness associated to each local node which, therefore, prevents the generation of spurious zero-energy modes, unlike nodal integration methods without stabilization. In order to overcome solution instabilities that are present in direct nodal integration, Taylor series expansions have been used, to serve as stabilization terms, as presented, respectively by Liu *et al.* (1985), for FEM, and by Liu *et al.* (1996) and Liu *et al.* (2007), for meshfree methods. While stable, the drawback of this stabilization technique is that it requires the calculation of high-order derivatives.

Therefore, there is still a clear need for an alternative modeling strategy that completely avoids all the issues associated with nodal integration. To fulfill such need, this paper presents a linearly integrated local meshfree numerical method.

The paper is organized as follows. The structural modeling is presented in Section 2, followed by the kinematic formulations in Section 3 and the modeling strategy in Section 4. Section 5 presents the local meshfree methods, while the local finite element methods are

presented in Section 6. Section 7 presents some numerical results, obtained for three standard benchmark problems, illustrating the accuracy, efficiency and robustness of the strategies adopted in the analysis. Finally, Section 8 presents the concluding remarks which include future developments.

2. Structural modeling

Let Ω be the domain of a structural body and Γ its boundary subdivided in Γ_u and Γ_t, with $\Gamma = \Gamma_u \cup \Gamma_t$, as represented in Figure 1. The general fundamental boundary value problem of linear elastostatics aims to determine the distribution of stresses σ, strains ε and displacements u, throughout the body, when it has constrained displacements $\bar{u}$, on Γ_u and it is loaded by an external system of distributed surface and body forces with densities denoted, respectively by $\bar{t}$, on Γ_t and b, in Ω.

The solution of these problem is a totally admissible elastic field that simultaneously satisfies the kinematic admissibility of the strains and the static admissibility of the stresses. Assuming that this solution exists, it can be shown that it is unique, provided linearity and stability of the material are admitted. Such is the Kirchhoff's theorem, on the uniqueness of solutions of the elastostatics boundary value problem, see Kirchhoff (1859). For the sake of generality, the solution of the posed problem is derived through the work theorem.

In the body's domain Ω consider a statically admissible stress field σ, which is any stress field that satisfies the equilibrium with the system of applied external forces which therefore satisfies

$$L^T \sigma + b = 0, \tag{2.1}$$

in the domain Ω, with boundary conditions

$$t = n\sigma = \bar{t}, \tag{2.2}$$

on the static boundary Γ_t, in which L is a matrix differential operator; t is the vector of traction components; t is the vector of the prescribed tractions and n is the matrix of the components of the unit outward normal to the boundary.

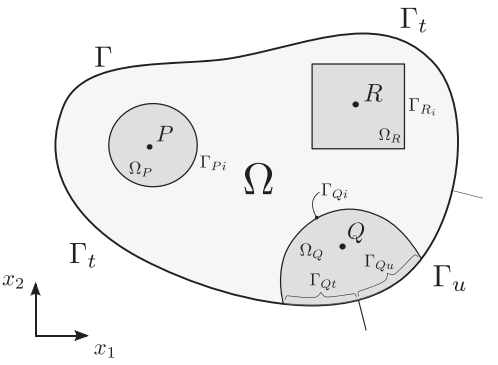

Figure 1.
Representation of the body's domain Ω, with boundary $\Gamma = \Gamma_u \cup \Gamma_t$

Note(s): The work theorem is defined in an arbitrary domain $\Omega_Q \in \Omega \cup \Gamma$, assigned to a reference point $Q \in \Omega_Q$, with boundary $\Gamma_Q = \Gamma_{Qi} \cup \Gamma_{Qt} \cup \Gamma_{Qu}$, in which Γ_{Qi} is the interior local boundary, and Γ_{Qt} and Γ_{Qu} are local boundaries that share the global boundaries, respectively the static boundary Γ_t and the kinematic boundary Γ_u; points P and R, have arbitrary local domains, respectively Ω_P and Ω_R

2.1 Local domain

In the domain Ω consider an arbitrary local domain Ω_Q, assigned to a reference point $Q \in \Omega_Q$, with local boundary $\Gamma_Q = \Gamma_{Qi} \cup \Gamma_{Qt} \cup \Gamma_{Qu}$, in which Γ_{Qi} is the interior local boundary, while Γ_{Qt} and Γ_{Qu} are local boundaries that share the global boundaries, respectively the static boundary Γ_t and the kinematic boundary Γ_u, as represented in Figure 1. The work theorem will be used as a local form that is valid in the arbitrary local domain Ω_Q. Due to its arbitrariness, this local domain $\Omega_Q \cup \Gamma_Q \in \Omega \cup \Gamma$ can be overlapping with other similar sub-domains that can be defined in the body.

2.2 The work theorem

The work theorem establishes an energy relationship, valid in an arbitrary local domain $\Omega_Q \in \Omega$, between two independent elastic fields that can be defined in the body which are, respectively, a statically admissible stress field that satisfies equilibrium with a system of external forces, and a kinematically admissible strain field that satisfies the compatibility with a set of constrained displacements. Derived as a weighted residual statement, see Oliveira and Portela (2016), the work theorem is expressed, in the local domain Ω_Q, as an integral form written compactly as

$$\int_{\Gamma_Q} t^T u^* \mathrm{d}\Gamma + \int_{\Gamma_Q} t^T u^* \mathrm{d}\Omega = \int_{\Gamma_Q} \sigma^T \varepsilon^* \, \mathrm{d}\Omega \tag{2.3}$$

in which the stress field σ and the strain field ε^* are not linked by any constitutive relationship and therefore, they are independent of each other, see Oliveira and Portela (2016). The statically admissible stress field σ can be any stress field that is in equilibrium with the system of applied external forces, therefore satisfying equations (2.1) and (2.2), which is not necessarily the stress field that the system of applied external forces actually introduces in the body. The kinematically admissible strain field ε^* can be any strain field defined in the body, generated by continuous displacements u^* with small derivatives, compatible with an arbitrary set of constraints specified on the kinematic boundary, which is not necessarily the strain field that actually settles in the body. Finally, the local domain ΩQ is any arbitrary sub-domain of the body, associated to the reference point Q, as represented in Figure 1, where the independent fields σ and ε^* are defined.

3. Kinematic formulations

Kinematic formulations consider, in the work theorem, a particular and convenient specification of the kinematically admissible strain field, leading thus to an equation of mechanical equilibrium that is used to generate the stiffness matrix of the numerical model.

3.1 Rigid-body displacement formulation

Bearing in mind the essential feature of the work theorem, which is the complete independence of the stress field σ and the strain field ε^*, the strain field can be conveniently defined by a rigid-body displacement that can be defined as

$$u^*(x) = c, \tag{3.1}$$

where c is a constant vector that conveniently leads to null strains that is

$$\varepsilon^*(x) = 0. \tag{3.2}$$

3.1.1 Local form. When the kinematically admissible strain field generated by the arbitrary rigid body displacement (3.1) is considered, the local form of the work theorem, equation (2.3), simply leads to the equation

$$\int_{\Gamma_Q - \Gamma_{Qt}} t \, d\Gamma + \int_{\Gamma_{Qt}} \bar{t} \, d\Gamma + \int_{\Omega_Q} b \, d\Omega = 0 \tag{3.3}$$

which states an integral form of mechanical equilibrium, of tractions and body forces, in the local domain Ω_Q. This equation expresses the local version of the basic Euler–Cauchy stress principle that is sometimes referred to as the defining principle of continuum mechanics (Truesdell and Toupin, 1960).

3.2 Virtual displacement formulation

Consider a kinematically admissible strain field generated by a virtual displacement, defined as an arbitrary variation of the actual displacement field, represented as

$$u^* = \delta u. \tag{3.4}$$

The assumed arbitrary variation of the actual displacement field vanishes on the kinematic boundary Γ_{Qu}, where the displacements of the problem are specified and therefore cannot be varied. The corresponding virtual strain generated by this virtual displacement can be represented as

$$\varepsilon^* = \delta\varepsilon. \tag{3.5}$$

3.2.1 Local form. When the kinematically admissible strain field of equations (3.4) and (3.5) is introduced in equation (2.3) of the work theorem, the following local form of virtual work is obtained

$$\int_{\Gamma_Q} t^T \delta u \, d\Gamma + \int_{\Omega_Q} b^T \delta u \, d\Omega = \int_{\Omega_Q} \sigma^T \delta\varepsilon \, d\Omega \tag{3.6}$$

which corresponds to the local form of the virtual displacement theorem.

In this paper, the local form of the virtual displacement formulation of the work theorem, equation (3.6), will be used only to set up a relationship between local formulations and the global formulation of the standard displacement assumed FEM.

4. Modeling strategy

Different formulations of numerical methods, which include meshfree and finite element methods, can be simply defined through the application of the work theorem, along with a proper and convenient kinematic formulation, in order to derive the equilibrium equations that are used to generate the stiffness matrix of each numerical model.

4.1 Defining the strain field

The kinematic formulation of the work theorem is carried out through the specification of an appropriate kinematically admissible strain field ε^*, as presented in Section 3. This paper considers the arbitrary rigid-body displacement formulation that leads to the local equilibrium equations (3.3), as well as the virtual displacement formulation that leads to the local equilibrium equations (3.6).

4.2 Defining the stress field

The modeling strategy, adopted to solve the actual elastic problem, considers that the stress field σ, required to satisfy the equilibrium with a system of external forces, is assumed as the stress field that actually settles in the body, when it is loaded by the actual system of external distributed surface and body forces, with the actual displacement constraints. Recall that the elastic field that actually settles in the body is the unique fully admissible elastic field that satisfies the given problem. Therefore, besides satisfying static admissibility, through equations (2.1) and (2.2), that is the same as satisfying equilibrium through equations (3.3) and (3.6) generated by the weak form (2.3) of the work theorem, this unique totally admissible elastic field also satisfies kinematic admissibility defined as

$$\varepsilon = Lu. \tag{4.1}$$

in the domain Ω, with boundary conditions

$$u = \bar{u}, \tag{4.2}$$

on the kinematic boundary Γ_u, in which the displacement u is assumed continuous with small derivatives, in order to allow for geometrical linearity of the strain field ε. Hence, equation (4.2), which specifies the constraints of the actual displacements, must be enforced in any numerical model, in order to provide a unique solution of the elastic problem.

For the sake of simplicity, this paper considers the formulation of meshfree and finite element numerical methods, in the absence of body forces. Consequently, the equations of equilibrium are always defined only on the boundary of the local domain.

5. Local meshfree numerical methods

The essential feature of meshfree numerical methods is that they perform the discretization of the problem domain and boundaries with a set of scattered field nodes that do not require any mesh for the approximation of the field variables. The moving least-squares (MLS) approximation is used in this paper. The basic MLS meshfree terminology, introduced by Atluri and Zhu (2000), along with a summary of the essential features of the MLS approximation, can be seen in Oliveira and Portela (2016).

In a meshfree discretization, each node is associated with its local domain, as schematically represented in Figure 2. In general, this local domain is a circular or rectangular region, centered at the respective node, where the rigid body displacement formulation of the work theorem is defined as a local form of mechanical equilibrium.

The local character of the MLS approximation is a direct consequence of the compact support of each node, where the respective shape functions are defined. Circular or rectangular local compact supports, centered at each node, can be used. The size of the compact support, in turn, sets out, in a neighborhood of a sampling point, the respective domain of definition of the MLS approximation at this point, as schematically represented in Figure 3.

The definition domain contains all the nodes whose MLS shape functions do not vanish at this sampling point. Therefore, the domain of influence of each node is the union of the MLS domains of definition of all points in the local domain of the node.

Finally, local mesh free formulations use a node-by-node calculation to generate, in the domain of influence of the local node, the respective rows of the global system of equations.

5.1 Local meshfree method (LMFM)

In the absence of body forces, the kinematic formulation of the local work theorem, equation (3.3), can be written simply as

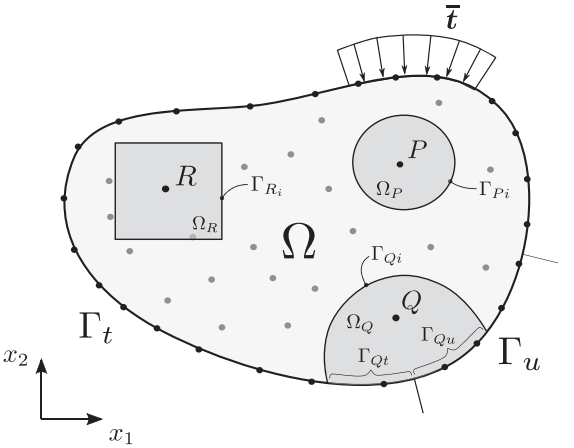

Figure 2.
Meshfree discretization of the global domain Ω, with boundary $\Gamma = \Gamma_u \cup \Gamma_t$

Note(s): Reference nodal points P, Q and R have associated corresponding local domains Ω_P, Ω_Q and Ω_R; in the local domain Ω_Q, with boundary $\Gamma_Q = \Gamma_{Qi} \cup \Gamma_{Qt} \cup \Gamma_{Qu}$, in which Γ_{Qi} is the interior local boundary, while $\Gamma_{Qt} \in \Gamma_t$ and $\Gamma_{Qu} \in \Gamma_u$, is defined the appropriate form of the work theorem, assigned to the node Q

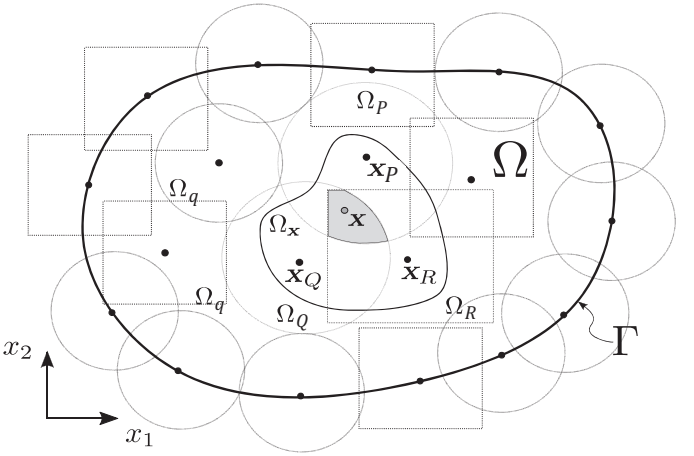

Figure 3.
Schematic representation of a meshfree discretization of the global domain Ω and boundary Γ, with a distribution of nodes

Note(s): Ω_P, Ω_Q and Ω_R represent the local compact supports of the corresponding nodes x_P, x_Q and x_R; Ω_x is the domain of definition, of the MLS approximation of the sampling point x, which is the set of nodes, in this case x_P, x_Q and x_R, whose compact support contains this sampling point

$$\int_{\Gamma_Q - \Gamma_{Qt}} t \, d\Gamma = - \int_{\Gamma_{Qt}} \bar{t} \, d\Gamma \tag{5.1}$$

which represents mechanical equilibrium of the boundary tractions of the local domain ΩQ, associated with the field node $Q \in \Omega Q$. Note that, although derived in an entirely different

way that does not make use of the work theorem, this equation corresponds to the model MLPG5, presented by Atluri and Shen (2002), here referred to as MLPG.

For a meshfree discretization of the body, the local meshfree method, symbolically referred to as LMFM, is used to compute the respective system of algebraic equations, in a node-by-node process, throughout integration of the corresponding local form (5.1) assigned to each node, with rectangular or circular local domains and numerical quadrature applied on each side, or quadrant, of the local domain, as schematically represented in Figure 4.

The MLS approximation of a displacement component $u^h(x)$ is performed in terms of the unknown nodal parameters $\widehat{u}_i$, see Oliveira and Portela (2016), as

$$u^h(x) = \sum_{i=1}^{n} \phi_i(x)\widehat{u}_i, \tag{5.2}$$

in which $\phi_i(x)$ is the shape function corresponding to the node x_i. Consequently, the approximation of the elastic field is also performed in terms of the unknown nodal parameters $\widehat{u}$, as

$$u = \begin{bmatrix} u^h(x) \\ v^h(x) \end{bmatrix} = \begin{bmatrix} \phi_1(x) & 0 & \dots & \phi_n(x) & 0 \\ 0 & \phi_1(x) & \dots & 0 & \phi_n(x) \end{bmatrix} \begin{bmatrix} \widehat{u}_1 \\ \widehat{v}_1 \\ \vdots \\ \widehat{u}_n \\ \widehat{v}_n \end{bmatrix} = \Phi\widehat{u} \tag{5.3}$$

and

$$\varepsilon = Lu = L\Phi\widehat{u} = B\widehat{u}, \tag{5.4}$$

in which geometrical linearity is assumed in the differential operator L and thus,

$$B = \begin{bmatrix} \phi_{1,1} & 0 & \dots & \phi_{n,1} & 0 \\ 0 & \phi_{1,2} & \dots & 0 & \phi_{n,2} \\ \phi_{1,2} & \phi_{1,1} & \dots & \phi_{n,2} & \phi_{n,1} \end{bmatrix}. \tag{5.5}$$

Stress and traction components are respectively approximated as

$$\sigma = D\,\varepsilon = DB\widehat{u}, \tag{5.6}$$

and

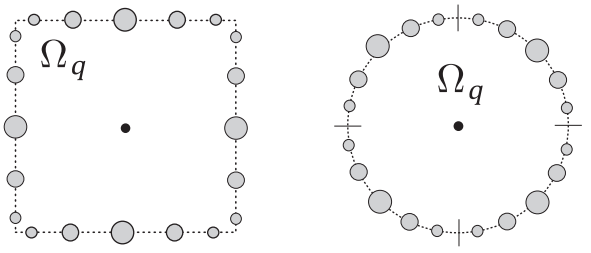

Figure 4. Schematic representation of numerical quadrature points, on each side, or quadrant, of local domains, for the computation of nodal equilibrium equations (5.1) in LMFM

$$t = n\sigma = nDB\widehat{u}, \tag{5.7}$$

in which D is the matrix of the elastic constants and n is the matrix of the components of the unit outward normal, defined as

$$n = \begin{bmatrix} n_1 & 0 & n_2 \\ 0 & 0 & n_1 \end{bmatrix} \tag{5.8}$$

Therefore, the MLS approximation of the local form (5.1) is carried out in terms of the unknown nodal parameters $\widehat{u}$, thus leading to the system of two linear equations

$$\int_{\Gamma_Q - \Gamma_{Qt}} n D B \widehat{u} \, d\Gamma = -\int_{\Gamma_{Qt}} \bar{t} \, d\Gamma \tag{5.9}$$

that can be written as

$$K_Q \widehat{u} = F_Q, \tag{5.10}$$

in which K_Q, denotes the stiffness matrix of the node Q, which is of the order $2 \times 2n$ (n represents the number of nodes of the influence domain of Q) given by

$$K_Q = \int_{\Gamma_Q - \Gamma_{Qt}} n D B \widehat{u} \, d\Gamma \tag{5.11}$$

and F_Q, denotes the force vector associated with the node Q, given by

$$F_Q = -\int_{\Gamma_{Qt}} \bar{t} \, d\Gamma \tag{5.12}$$

For a problem with a total of N nodes, in which M is the number of interior and static-boundary nodes, the assembly of equations (5.10) for all M nodes leads to the $2M \times 2N$ system of equations

$$K\widehat{u} = F \tag{5.13}$$

Finally, the remaining equations are obtained from the N–M nodes on the kinematic boundary. For each of these nodes, a direct interpolation method, first presented by Liu and Yan (2000), is used to impose the boundary condition as

$$u_k^h(x_j) = \sum_{i=1}^{n} \phi_i(x_j) \widehat{u}_{i,k} = \bar{u}_k, \tag{5.14}$$

with $k = 1,2$, where $\bar{u}_k$ is the specified nodal displacement component. Equations (5.14) are directly assembled into the global system of equations (5.13).

It is important to note that, the line integration carried out only on the boundary of the local domain, in equation (5.1), to build the respective nodal stiffness matrix of LMFM, is computationally much more efficient than other meshfree methods that use domain integration, as is the case of the EFG method, presented by Belytschko *et al.* (1994), or the MLPG1, MLPG3 and MLPG6 methods presented by Atluri *et al.* (Atluri and Shen, 2002). The higher efficiency of LMFM is clearly evident in numerical results.

5.2 Integrated local meshfree method (ILMFM)

In the absence of body forces, general numerical methods can be effectively formulated through an integrated local form of the work theorem which, in the simplest linear case, leads to a point–wise discrete form that improves the accuracy and the computational efficiency, as numerical results clearly demonstrate. Hence, assuming a linear variation of tractions along each boundary segment of the local domain, the local integral form of equilibrium can be exactly evaluated with a single quadrature point, centered on each segment of the boundary. In this case, equation (5.1) simply leads to.

$$\frac{L_i}{n_i}\sum_{j=1}^{n_i} t_{x_j} = -\frac{L_t}{n_t}\sum_{k=1}^{n_t} \bar{t}_{x_k}, \tag{5.15}$$

in which n_i and n_t denote the total number of integration points, or boundary segments, defined on, respectively the interior local boundary $\Gamma_{Qi} = \Gamma_Q - \Gamma_{Qt} - \Gamma_{Qu}$, with length L_i, and the local static boundary Γ_{Qt}, with length L_t. This integrated equation, which leads to the formulation of the integrated local meshfree method, symbolically referred to as ILMFM, represents a point–wise discrete form of mechanical equilibrium of tractions, evaluated at a set of points on the boundary of the local domain Ω_Q.

Consider a meshfree discretization of the body. Then, ILMFM is used to compute the respective system of algebraic equations, in a node-by-node process, throughout traction evaluation at each central point of the boundary segments of the corresponding integrated local form (5.15) assigned to each node, with rectangular or circular local domains. Figure 5 schematically represents these local domains with four boundary segments and one integration point on each segment (side, or quadrant) of the respective local domain.

Discretization of the integrated local form (5.15) is carried out with the MLS approximation, in terms of the unknown nodal parameters $\widehat{u}$, thus leading to the system of two linear algebraic equations

$$\frac{L_i}{n_i}\sum_{j=1}^{n_i} n_{x_j} D B_{x_j} \widehat{u} = -\frac{L_t}{n_t}\sum_{k=1}^{n_t} \bar{t}_{x_k} \tag{5.16}$$

that can be written as

$$KQ\widehat{u} = FQ, \tag{5.17}$$

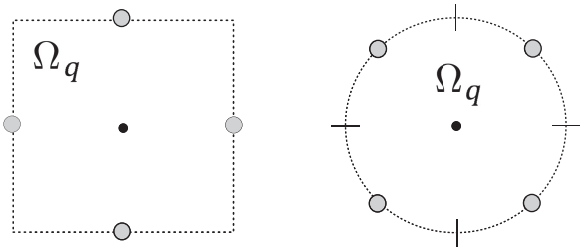

Figure 5. Schematic representation of rectangular and circular local domains

Note(s): One point on each side, or quadrant, of the local domain, for the computation of the integrated local form (5.15) of ILMFM

in which K_Q, the nodal stiffness matrix associated with the node Q, is a $2 \times 2n$ matrix (n is the number of nodes included in the domain of influence of the node Q that is the union of the MLS domains of definition of all integration points in the local domain Ω_Q) given by

$$K_Q = \frac{L_i}{n_i} \sum_{j=1}^{n_i} n_{x_j} D B_{x_j} \tag{5.18}$$

and F_Q is the respective force vector given by

$$F_Q = -\frac{L_t}{n_t} \sum_{k=1}^{n_t} \bar{t}_{x_k}. \tag{5.19}$$

Consider that the problem has a total of N nodes. Assembling equation (5.17) for all M interior and static-boundary field nodes leads to the global system of $2M \times 2N$ equations

$$K\widehat{u} = F. \tag{5.20}$$

Finally, the remaining equations are obtained from the $N - M$ boundary nodes on the kinematic boundary. For a node on the kinematic boundary, a direct interpolation method is used to impose the boundary condition as

$$u_k = \Phi_k \widehat{u} = \bar{u}_k, \tag{5.21}$$

with $k = 1,2$, where $\bar{u}_k$ is the specified nodal displacement component. Equation (5.21) is directly assembled into the global system of equation (5.20).

It can be easily anticipated higher computational efficiency and improved accuracy of results of ILMFM, when compared against results of LMFM. As a matter of fact, while in LMFM the computation of the nodal stiffness matrix, in equation (5.11), is carried out through standard numerical quadrature, with several integration points on each side of the local boundary, which is a time consuming process, in ILMFM it is effectively computed, in equations (5.18), with only one integration point on each segment of the local boundary, which basically implies a reduction of the processing time to run the analysis. In addition, the linear reduced integration performed by ILMFM induces a reduction of the stiffness that is accompanied by an improvement of the accuracy, with no instabilities. This accuracy improvement, generated by the reduced integration, has been already used in the standard displacement assumed FEM to prevent locking, Zienkiewicz *et al.* (Zienkiewicz and Taylor, 1983).

The compact support and the local domain of each node of the meshfree discretization are the essential features that lead to the independence of the equilibrium equations generated in each local domain. Note that this independence is an important feature of local meshfree formulations, which allows the use of conveniently defined local domains, simultaneously modeled with different formulations, or the use of enrichment of a particular nodal stiffness matrix without increasing the nodal degrees of freedom.

5.3 Parameters of the meshfree discretization

For each node of a meshfree discretization, the size $r_{\Omega s}$ of the compact support Ω_s, where shape functions are defined, and the size $r_{\Omega q}$ of the local domain Ω_q, where the work theorem is defined, are very important parameters that can affect the performance of the solution of a numerical application. For a generic node i, of a meshfree discretization, these parameters can be defined, respectively as

$$r_{\Omega s} = \alpha_s c_i \tag{5.22}$$

$$r_{\Omega q} = \alpha_q c_i, \tag{5.23}$$

in which c_i represents the distance of the node i, to the nearest neighboring node, while α_s and α_q are constant parameters that must be defined in any application.

6. Local finite element numerical methods

Consider a finite element discretization of the body. While the standard displacement assumed FEM can be derived from a global form of the work theorem that extends to the whole domain of the body, local formulations are derived from a local form of the work theorem, defined in appropriate local regions, around each node of the finite element mesh.

Let Ω_x be the finite element, with n nodes $x_i \in \Omega$, $i = 1,2, \ldots, n$, that contains the sampling point $x \in \Omega_x$. To approximate the displacement component $u(x)$ in Ω_x, over the n element nodes where the unknown nodal displacements $\widehat{u}_i$ are defined, the finite-element approximation is given by

$$u^h(x) = \sum_{i=1}^{n} \phi_i(x)\widehat{u}_i, \tag{6.1}$$

in which $\phi_i(x)$ is the shape function corresponding to the node x_i. The finite element shape functions are nodal interpolants that is $\phi_i(x_j) = \delta_{ij}$. Since $\phi_i(x)$ vanishes for x not in the finite element, the local character of the approximation is preserved. Hence, the variables of the elastic field are approximated, at a sampling point x, in terms of the nodal unknowns $\widehat{u}$, respectively as

$$u = \begin{bmatrix} u^h(x) \\ v^h(x) \end{bmatrix} = \begin{bmatrix} \phi_1(x) & 0 & \ldots & \phi_n(x) & 0 \\ 0 & \phi_1(x) & \ldots & 0 & \phi_n(x) \end{bmatrix} \begin{bmatrix} \widehat{u}_1 \\ \widehat{v}_1 \\ \vdots \\ \widehat{u}_n \\ \widehat{v}_n \end{bmatrix} = \Phi\widehat{u} \tag{6.2}$$

and

$$\varepsilon = L\,u = L\,\Phi\,\widehat{u} = B\,\widehat{u}, \tag{6.3}$$

in which geometrical linearity is assumed in the differential operator L and thus,

$$B = \begin{bmatrix} \phi_{1,1} & 0 & \ldots & \phi_{n,1} & 0 \\ 0 & \phi_{1,2} & \ldots & 0 & \phi_{n,2} \\ \phi_{1,2} & \phi_{1,1} & \ldots & \phi_{n,2} & \phi_{n,1} \end{bmatrix}. \tag{6.4}$$

where $()_{,k} = \partial()/\partial x_k$. Stress and traction components are respectively approximated as

$$\sigma = D\,\varepsilon = DB\,\widehat{u}, \tag{6.5}$$

and

$$t = n\sigma = nDB\widehat{u}, \tag{6.6}$$

in which D is the matrix of the elastic constants and n is the matrix of the components of the unit outward normal, defined as

$$n = \begin{bmatrix} n_1 & 0 & n_2 \\ 0 & 0 & n_1 \end{bmatrix} \tag{6.7}$$

In a local formulation, each node of the finite element mesh discretization is associated with its local domain, as schematically represented in Figure 6, which is a local region, defined around the assigned node of the mesh, where the equilibrium equations are generated by the work theorem. For each node of the mesh, its local region is simply the set of finite elements that share this node. Consequently, overlapping of neighboring local domains, as schematically represented in Figure 6, is a feature allowed in local formulations of FEM.

Regarding approximation, local formulations associate to each node of the finite element mesh discretization a global basis or shape function of compact support, as schematically represented in Figure 7, where the finite element approximation is defined with a local character. This compact support is defined around the respective node of the finite element mesh as the set of finite elements that share this node and, therefore, is coincident with the local domain of the respective node, where the equilibrium equations resulting from the work theorem are defined.

At an arbitrary sampling point, in a finite element mesh discretization of the body, the respective domain of definition of the finite element approximation contains all the nodes whose shape functions do not vanish at the sampling point which obviously is the finite element that contains the sampling point, as schematically represented in Figure 8.

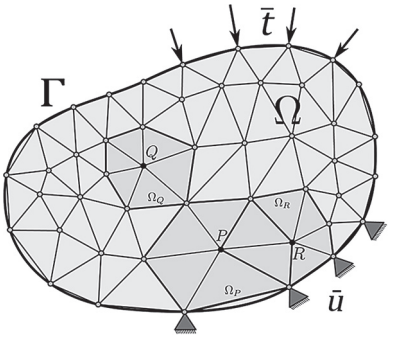

Figure 6.
Schematic representation of the local domain Ω_Q, associated with the node $Q \in \Omega_Q$, of a constant strain finite element mesh

Note(s): Local domains $\Omega_P \in \Omega_P$ and $\Omega_R \in \Omega_R$, associated with the nodes, respectively P and R, are overlapping

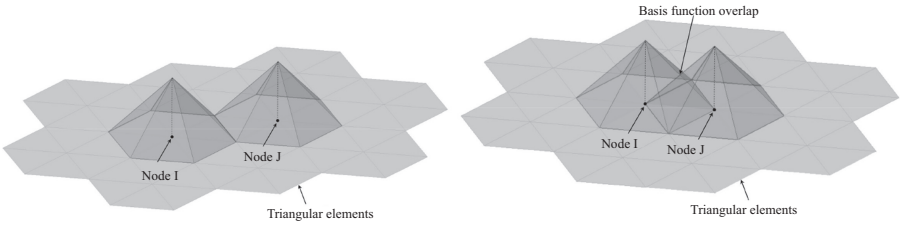

Non overlapping **(a)** Overlapping **(b)**

Figure 7.
Global basis or shape function of compact support, associated to each node of the finite element mesh

Local formulations of the finite element method use a node-by-node calculation to generate the rows of the global system of equations, while the global formulation uses the standard element-by-element stiffness calculation, that is assembled into the global stiffness matrix.

6.1 Local finite element method (LFEM)

In the absence of body forces, the local form of the kinematic formulation of the work theorem, equation (3.3), can be written simply as

$$\int_{\Gamma_Q - \Gamma_{Qt}} t \, d\Gamma = - \int_{\Gamma_{Qt}} \bar{t} \, d\Gamma \tag{6.8}$$

which represents mechanical equilibrium of boundary tractions of the local domain Ω_Q, associated with the node $Q \in \Omega_Q$.

For a finite element mesh discretization of the body, the local finite element method, symbolically referred to as LFEM, is used to compute the respective system of algebraic equations, in a node-by-node process. Hence, for each node of the mesh, the corresponding local form (6.8) is integrated along the boundary of the respective local domain. It is important to note that LFEM is not restricted to any particular type of finite element.

Consider that n_i and n_t represent the total number of finite elements that span, respectively the interior local boundary $\Gamma_{Qi} = \Gamma_Q - \Gamma_{Qt} - \Gamma_{Qu}$ and the local static boundary Γ_{Qt}. Then the equilibrium equation (6.8) can be written as

$$\sum_{j=1}^{n_i} \int_{\Gamma_Q - \Gamma_{Qt}} t_j \, d\Gamma = - \sum_{k=1}^{n_t} \int_{\Gamma_{Qt}} \bar{t}_k \, d\Gamma \tag{6.9}$$

Discretization of this equation is carried out with the finite element approximation, equations (6.2)–(6.6), in terms of the unknown nodal displacements u, thus leading to the system of two linear equations

$$K_Q u = F_Q, \tag{6.10}$$

in which K_Q, the nodal stiffness matrix associated with the node Q, is a $2 \times 2n$ matrix (n is the number of nodes included in the compact support of the node Q) given by

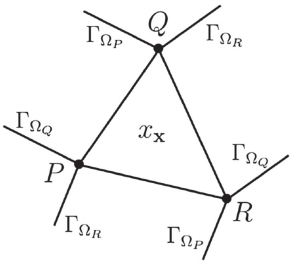

Note(s): The respective domain of definition of the finite element approximation contains the element nodes P, Q and R, whose shape functions do not vanish at the sampling point. Note that local domains Ω_P, Ω_Q and Ω_R, associated with the corresponding nodes P, Q and R, simultaneously contain the sampling point, that is $x \in \Omega_P$, $x \in \Omega_Q$ and $x \in \Omega_R$

Figure 8.
Schematic representation of a sampling point x, in a constant strain triangular finite element

$$K_Q = \sum_{j=1}^{n_i} \int_{\Gamma_Q - \Gamma_{Qt}} n_j D B_j \mathrm{d}\Gamma \tag{6.11}$$

and F_Q, is the force vector associated with the node Q, given by

$$F_Q = -\sum_{k=1}^{n_t} \int_{\Gamma_{Qt}} \bar{t}_k \, \mathrm{d}\Gamma. \tag{6.12}$$

Consider that the discretization of the body has a total of N nodes. Then, assembling equations (6.10) for all M interior and static-boundary nodes leads to the global system of $2M \times 2N$ equations

$$Ku = F. \tag{6.13}$$

Finally, the remaining equations are obtained from the $N - M$ nodes on the kinematic boundary. For a node on the kinematic boundary, the respective boundary condition can be imposed as

$$u_k(x_j) = \bar{u}_k, \tag{6.14}$$

with $k = 1,2$, where $\bar{u}_k$ is the specified nodal displacement component. Equation (6.14) is directly assembled into the global system of equation (6.13).

It is important to note the higher computational efficiency of the local formulation LFEM, over the standard FEM, whenever the discretization is carried out with higher-order finite elements. This is a consequence of the simple line integration of LFEM, carried out only on the boundary of the local domain, as represented in equation (6.9), against the two-dimensional integration of the finite element stiffness of the standard FEM.

6.2 Integrated local finite element method (ILFEM)

In the absence of body forces, general numerical methods can be effectively formulated through an integrated local form of the work theorem with rigid-body displacements which, in the simplest linear case, leads to a point–wise discrete form that improves the higher computational efficiency of LFEM.

When a linear variation of tractions is assumed, along each boundary segment of the local domain, the local form of the work theorem can be exactly integrated with one quadrature point, centered on each segment of the boundary. Thus, when this linear integration process is considered, equation (6.8) can be written simply as

$$\frac{L_i}{n_i} \sum_{j=1}^{n_i} t_{x_j} + \frac{L_t}{n_t} \sum_{k=1}^{n_t} \bar{t}_{x_k} = 0, \tag{6.15}$$

in which n_i and n_t represent the total number of integration points, or segments, defined on, respectively the interior local boundary $\Gamma_{Qi} = \Gamma_Q - \Gamma_{Qt} - \Gamma_{Qu}$, with length L_i, and the local static boundary Γ_{Qt}, with length L_t. This integrated equation represents a point–wise discrete form of boundary tractions at a set of $n_i + n_t$ integration points of the local domain Ω_Q, assigned to the node $Q \in \Omega_Q$.

For a finite element discretization, the integrated local finite-element method, symbolically referred to as ILFEM, is used to compute the respective system of algebraic equations, in a node-by-node process. For each node of the finite element mesh, the corresponding integrated

local form (6.15) is evaluated at the integration points of the respective local domain, which are defined at the center of the boundary side of each finite element of the local domain. It is important to note that ILFEM is not restricted to any sort of finite element type.

Discretization of the equilibrium equations (6.15) is carried out with the finite element approximation, equations (6.2)–(6.6), defined in terms of the unknown nodal displacements u, thus leading to a system of two linear equations that can be written as

$$K_Q u = F_Q, \tag{6.16}$$

in which K_Q, the nodal stiffness matrix associated with the field node Q, is a $2 \times 2n$ matrix (n is the number of nodes included in the compact support of the node Q) given by

$$K_Q = \frac{L_i}{n_i} \sum_{j=1}^{n_i} n_{x_j} D B_{x_j} \tag{6.17}$$

and F_Q, is the load vector associated with the node Q, given by

$$F_Q = -\frac{L_t}{n_t} \sum_{k=1}^{n_t} \int_{\Gamma_{Qt}} \bar{t}_{x_k}. \tag{6.18}$$

Consider that the discretization of the body has a total of N nodes. Then, assembling equation (6.16) for all M interior and static-boundary nodes leads to the global system of $2M \times 2N$ equations

$$Ku = F. \tag{6.19}$$

Finally, the remaining equations are obtained from the $N - M$ nodes on the kinematic boundary. For a node on the kinematic boundary, the respective boundary condition can be imposed as

$$u_k(x_j) = \bar{u}_k, \tag{6.20}$$

with $k = 1, 2$, where $\bar{u}_k$ is the specified nodal displacement component. Equation (6.20) is directly assembled into the global system of equation (6.19).

It is quite important to note the higher computational efficiency of the integrated local formulation of ILFEM, when compared against the local formulation of LFEM, whenever the discretization is carried out with higher-order finite elements. In effect, while in ILFEM the computation of the nodal stiffness matrix, through equation (6.17), is performed with one integration point on each element, in LFEM it is carried out, through equation (6.11), with standard numerical quadrature with several integration points, which is a time-consuming process. Furthermore, the reduced integration performed by ILFEM decreases the stiffness of the local node, which leads to an increase in the solution accuracy. This behavior, also present in the integrated local meshfree method, is obviously an advantage of the local formulation of ILFEM over the global standard formulation of FEM.

6.3 Constant strain triangular mesh

Consider now the discretization of the body with a mesh of constant strain triangular finite elements. In this case, local formulations may become not as advantageous as in the case of a mesh with higher-order finite elements, since the constant strain triangular finite element already leads to a constant stiffness matrix, therefore free of integration, in the standard FEM.

The first consequence of adopting such simple kind of discretization, with a mesh of constant strain triangular finite elements, is that both local formulations of LFEM and ILFEM generate exactly the same system of algebraic equations, provided the same finite element mesh is used. In effect, for the node Q, the respective nodal stiffness matrix generated by LFEM, equation (6.11), can be written as

$$K_Q = \sum_{j=1}^{n_i} \int_{\Gamma_Q - \Gamma_{Qt}} n_j \, D \, B_j \mathrm{d}\Gamma = \sum_{j=1}^{n_i} L_j \, n_j \, D \, B_j, \tag{6.21}$$

in which n_i is the total number of finite elements of the compact support that span the interior local boundary $\Gamma_{Qi} = \Gamma_Q - \Gamma_{Qt} - \Gamma_{Qu}$, with linear segments of length L_j and unit outward normal n_j.

On the other hand, for the same node Q, the respective nodal stiffness matrix generated by ILFEM, equations (6.17), with one integration point on each linear segment of length L_j, such that $L_i = \sum_{j=1}^{n_i} L_j$, of the interior local boundary defined by the finite elements of the compact support, can be written as

$$K_Q = \frac{L_i}{n_i} \sum_{j=1}^{n_i} n_{x_j} \, D \, B_{x_j} = \sum_{j=1}^{n_i} L_j \, n_j \, D \, B_j \tag{6.22}$$

which is absolutely identical to equation (6.21), and therefore proves that the same system of algebraic equation is generated by LFEM and ILFEM.

The second consequence, of adopting a finite element mesh discretization of constant strain triangles, is that the system of algebraic equations generated by the local formulations of LFEM and ILFEM is absolutely identical to the one generated by the standard FEM, provided the same linear triangular finite element mesh is used. This can be easily shown, for instance, with the case of LFEM, in two steps, as follows.

In the first step, consider that the equilibrium of boundary tractions, of the local domain Ω_Q, in equation (6.8), can be computed either in a segment by-segment resultant process, as represented in equation (6.9), or throughout the resultant of the equivalent nodal forces. These two processes of equilibrium enforcement, in the reference local domain, are absolutely equivalent, as schematically represented in Figure 9.

Hence, in the second step, consider the equivalent nodal forces of the boundary tractions, of the local domain Ω_Q. In the absence of body forces, the local virtual displacement

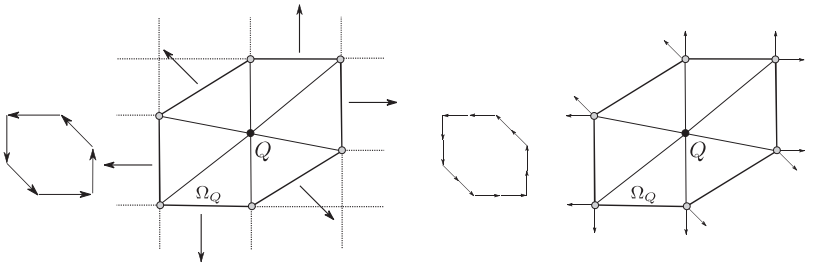

Figure 9. Schematic representation of the equilibrium of boundary tractions of the local domain Ω_Q, associated with the field node $Q \in \Omega_Q$, in a constant strain finite element mesh

Note(s): (a) computed in a segment-by-segment resultant process; (b) computed throughout the equivalent nodal forces

formulation of the work theorem, equations (3.6), can be used to compute these equivalent nodal forces as

$$\int_{\Gamma_Q} t^T \delta u \, d\Gamma = \int_{\Omega_Q} \sigma^T \delta\varepsilon \, d\Omega. \tag{6.23}$$

For the finite element approximation, equations (6.2)–(6.6), the arbitrary virtual variations, defined in terms of the element nodal displacements $\widehat{u}$, respectively as

$$\delta u = \Phi \delta\widehat{u} \tag{6.24}$$

and

$$\delta\varepsilon = L\,\delta\widehat{u} = L\,\Phi\delta\widehat{u} = B\,\delta\widehat{u}, \tag{6.25}$$

eventually lead to the final equation

$$\int_{\Gamma_Q} \Phi^T t \, d\Gamma = \int_{\Omega_Q} B^T D B u \, d\Omega. \tag{6.26}$$

For each finite element of the local domain Ω_Q, the left-hand side of equation (6.26) represents the equivalent nodal forces of the boundary tractions, obviously with null components for the node Q.

Therefore, since the equilibrium of boundary tractions of the local domain Ω_Q, represented by equation (6.8), computed in a segment-by-segment resultant process, as represented in equation (6.9), is identical to the resultant of the equivalent nodal-forces, represented by the left-hand side of equation (6.26), that is

$$\int_{\Gamma_Q} t \, d\Gamma = \sum_{j=1}^{n_i} \int_{\Gamma_Q} t_j \, d\Gamma \equiv \sum_{j=1}^{n_i} \int_{\Gamma_Q} \Phi^T t_j \, d\Gamma, \tag{6.27}$$

it can be concluded that the local stiffness matrix of equation (6.8) that is equation (6.11), is equivalent to the right-hand side of equation (6.26) that is

$$K_Q = \sum_{j=1}^{n_i} \int_{\Gamma_Q} n_j D B_j d\Gamma \equiv \sum_{j=1}^{n_i} \int_{\Omega_Q} B_j^T D B_j d\Omega, \tag{6.28}$$

which represents the stiffness matrix of the standard FEM. This proves that local formulations LFEM and ILFEM generate a system of algebraic equations that is equivalent to the one generated by the global formulation of the standard FEM, provided the same linear triangular finite element mesh is used. Therefore, both global and local formulations of the finite element method lead to the same solution, for the same triangular finite element mesh discretization. This means that whenever these formulations of the finite element method consider the same triangular finite element approximation, they lead to the same solution accuracy which only depends on the discretization used.

An important remark, regarding the computational efficiency of the local formulations LFEM and ILFEM, whenever a constant strain triangular finite element mesh discretization is considered, must be emphasized. Local formulations generate the global stiffness matrix of the body, in a node-by-node calculation, as presented in equations (6.21) and (6.22), for the node Q. Consequently, for each finite element of the triangular mesh, the constant strain of the element is evaluated three times, in order to compute the element contribution for the

corresponding nodal stiffness, as schematically represented in Figure 8, for the element nodes P, Q and R. This makes local formulations LFEM and ILFEM, possibly less efficient than the standard FEM, where the stiffness of each finite element is computed only once, although it must be assembled in the global stiffness matrix of the body, row by row.

The compact support and the local domain, of each node of the finite element mesh, are the key properties that lead to the independence of the equilibrium equations generated in each local domain. This independence is a feature of extremely importance of local finite element formulations that allows the use of local domains, simultaneously modeled with different formulations, or the use of enrichment of a particular nodal stiffness matrix, without increasing the nodal degrees of freedom, in conveniently defined local domains.

7. Numerical results

This section presents some numerical results to illustrate the accuracy and efficiency of the new formulations, both the local and the integrated local, meshfree and finite element numerical methods.

The norms can be used for error estimation in displacement and energy. These error norms can be defined, respectively as

$$\|u\| = \left[\int_{\Omega} (u - u_{\text{exact}})^T (u - u_{\text{exact}}) \mathrm{d}\Omega\right]^{1/2} \tag{7.1}$$

And

$$\|\varepsilon\| = \left[\int_{\Omega} (\varepsilon - \varepsilon_{\text{exact}})^T D(\varepsilon - \varepsilon_{\text{exact}}) \mathrm{d}\Omega\right]^{1/2}, \tag{7.2}$$

in which u and ε represent, respectively the numerical results of displacement and strain, whereas u_{exact} and $\varepsilon_{\text{exact}}$ represent the corresponding values of the exact solution.

7.1 Benchmark 1 – patch test

As a first benchmark problem, consider the standard patch test, an analysis of a rectangular plate loaded by a uniform normal traction applied on the top edge, with proper displacement constraints on the bottom edge, as represented in Figure 10. The plate is assumed in a plane stress condition and the material parameters are Young's modulus $E = 1.0$ and the Poisson's

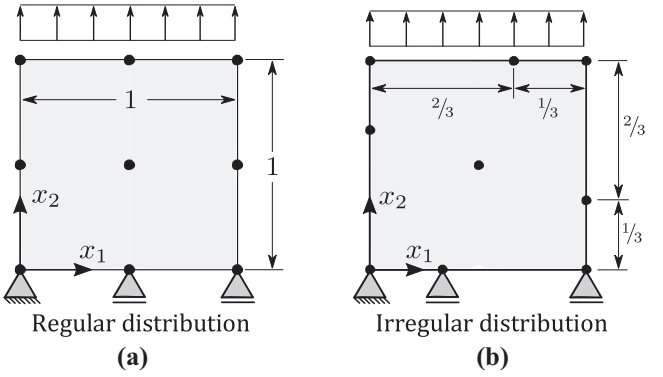

Figure 10.
The patch test, analysis of a rectangular plate under a uniform normal traction discretized with two nodal distributions

ratio $\nu = 0.25$. The plate is discretized with nine nodes, arranged in two nodal configurations in which one is regular and the other is irregular, as shown in Figure 10. Rectangular local integration domains Ωq were considered. On each side of the local domain, LMFM was applied with eight Gauss-quadrature points, while ILMFM was applied with one integration point at the center of the segment.

The results obtained, represented in Figure 11, are a linear displacement on lateral edges and a constant displacement on the top edge; the normal stress in the loading direction is constant and there is no shear stress in the plate, as expected.

7.2 Benchmark 2 – cantilever-beam

As a second benchmark problem, consider a cantilever beam with dimensions $L \times D$ and with unit depth, subjected to a parabolic traction at the free end, as shown in Figure 12. The beam is assumed in a plane stress state and the parabolic traction is defined as

$$\bar{t}_2(x_2) = -\frac{P}{2I}\left(\frac{D^2}{4} - x_2^2\right), \tag{7.3}$$

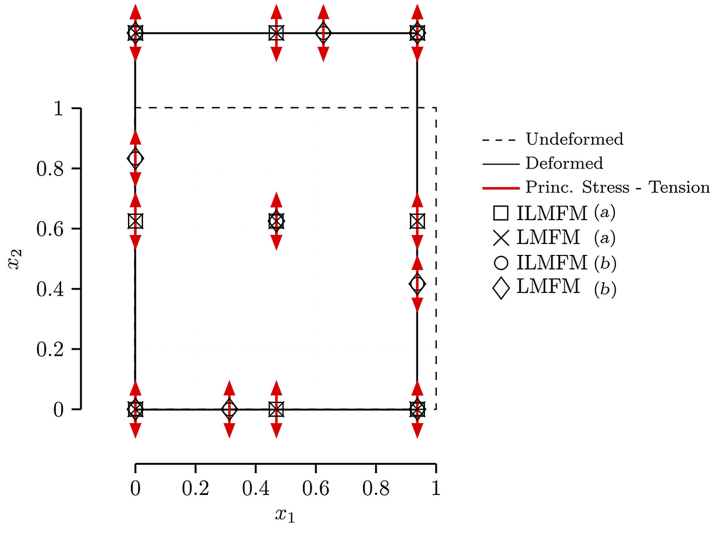

Figure 11.
Results of the patch test are a linear displacement on lateral edges, a constant displacement on the top edge, a constant normal stress in the loading direction and no shear stress

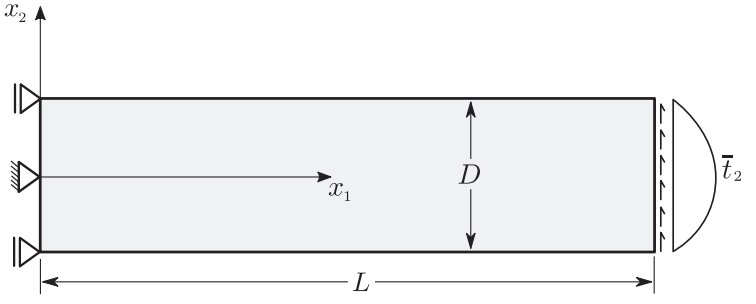

Figure 12.
Timoshenko's cantilever beam

where $I = D^3/12$ is the moment of inertia. Material properties of the cantilever beam are taken as Young's modulus $E = 3.0 \times 10^7$ and the Poisson's ratio $\nu = 0.3$ and the beam dimensions are $D = 12$ and $L = 48$. The shear force is $P = 1{,}000$.

7.3 Meshfree discretization

In order to improve the accuracy of a meshfree numerical model, the discretization requires a proper refinement of $r_{\Omega s}$ and $r_{\Omega q}$, through the specification of parameters α_s and α_q defined in equations, respectively, (5.22) and (5.23). In general, the discretization parameters are considered, respectively as $\alpha_s > 1.0$ and $\alpha_q < 1.0$. As a matter of fact, for a small size $r_{\Omega s}$, the algorithm of the MLS approximation may be singular and the shape function cannot be constructed, because there are not enough nodes in Ω_s for interpolating. On the other hand, local domains Ω_q can be overlapping; however, the size $r_{\Omega q}$ should ensure that the local domain, of internal nodes, is entirely within the solution domain, without intersecting the boundary of the body.

To obtain the appropriate values of the discretization parameters, for the benchmark problem, a parametric analysis was carried out with four regular discretizations of the cantilever beam, with $33 \times 5 = 165$, $65 \times 9 = 585$, $97 \times 13 = 1{,}261$ and $129 \times 17 = 2{,}193$ nodes, from which, the one with 165 nodes is represented in Figure 13. The results obtained for this parametric analysis, represented in Figure 14, clearly show that the optimum values of the discretization parameters are $\alpha_s = 4.5$ and $\alpha_q = 0.5$ which, therefore, are the values considered for the applications presented in this paper.

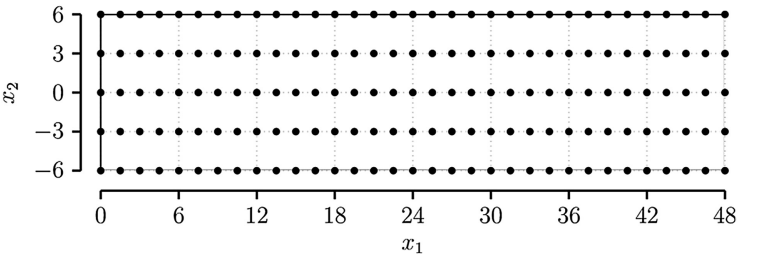

Figure 13.
Regular nodal distribution of the cantilever-beam discretization with $33 \times 5 = 165$ nodes

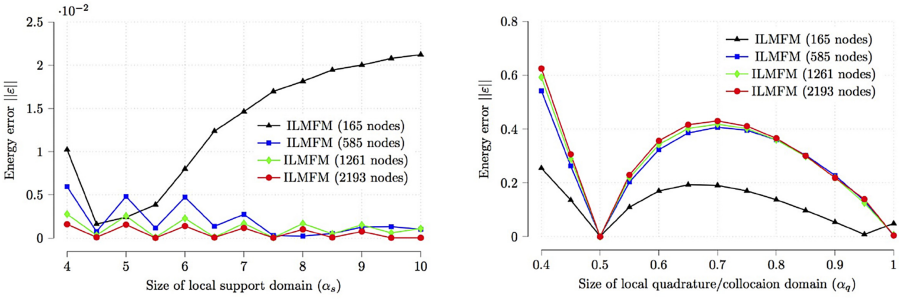

Figure 14.
Analysis of the meshfree discretization parameters α_s and α_q

Note(s): α_s and α_q are defined in equations, respectively (5.22) and (5.23), carried out with four regular discretizations of the cantilever beam, with $33 \times 5 = 165$, $65 \times 9 = 585$, $97 \times 13 = 1{,}261$ and $129 \times 17 = 2{,}193$ nodes

Rectangular local domains Ω_q were considered to compute the equilibrium equations. While in the case of ILMFM, integration was performed with 1 point, centered on each side of Ω_q, in the case of LMFM, integration was carried out with 10 points of Gauss quadrature, placed along each boundary of Ω_q, as schematically represented, respectively in Figures 5 and 4. A first-order polynomial basis was used in the MLS approximation of both meshfree methods.

To solve the benchmark problem, a regular nodal distribution, represented in Figure 13, was considered with a discretization of $33 \times 5 = 165$ nodes.

7.4 Meshfree displacement and stress

Displacements obtained with LMFM and ILMFM, presented in Figure 15, show very good agreement with corresponding results of the exact solution. Error norms in displacement $u = 6.69 \times 10^{-5}$ and in energy $\epsilon = 1.58 \times 10^{-3}$ were obtained with ILMFM for this relatively coarse nodal configuration. As shown in Figure 16, stresses, computed at the center of the

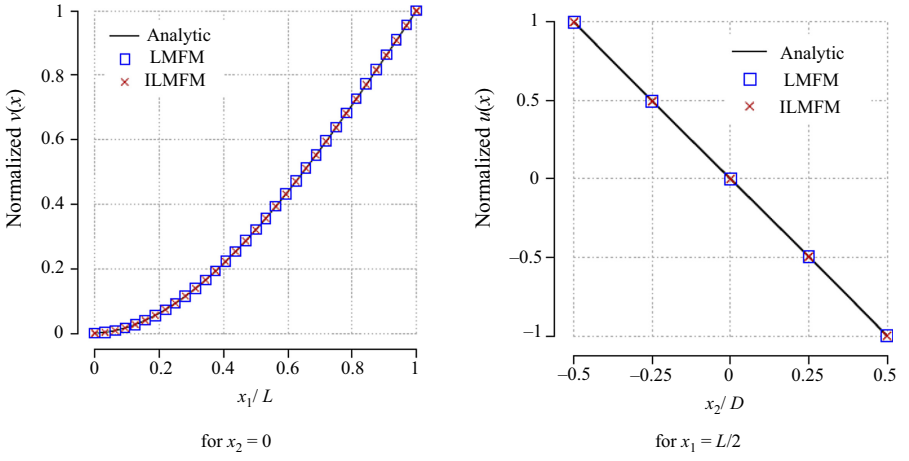

Figure 15. Normalized displacements of the cantilever-beam discretization with $33 \times 5 = 165$ nodes

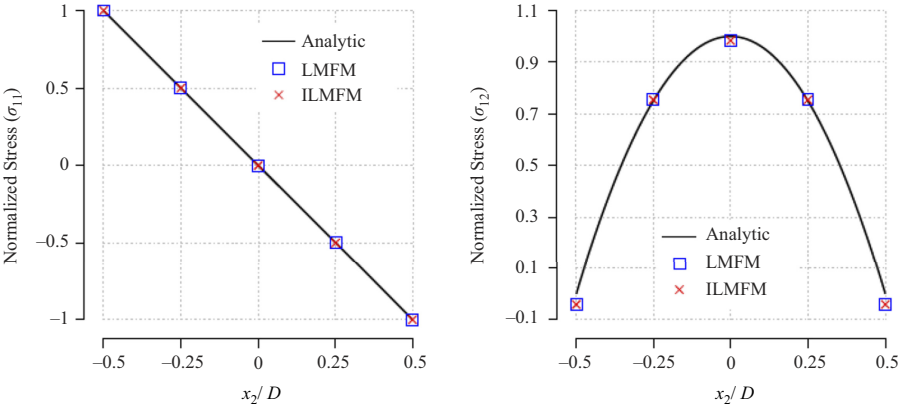

Figure 16. Stress distribution for $x_1 = L/2$ and $x_2 \in [-D/2, D/2]$ of the cantilever-beam discretization with $33 \times 5 = 165$ nodes

beam that is $x_1 = L/2$ and $x_2 \in [-D/2, D/2]$, also present very good agreement with corresponding results of the exact solution.

7.5 Performance of ILMFM

The highly relevant performance of ILMFM is a key feature of this new numerical method. Linear integration is considered with one central point on any segment of the local boundary. Additional points can be considered by subdividing the boundary segment. This paper considers identical segments, on each side of the local domain, which leads to equally spaced integration points.

Therefore, it is important to assess the performance of the method, as a function of the number of integration points, or segments, defined on each side of the local domain. Figure 17 shows the behavior of the error norm in energy ε of ILMFM, in terms of the number of integration points, for the discretization of $33 \times 5 = 165$ nodes; for comparison, the error norm of LMFM, computed with 10 Gauss integration points on each side of the local domain, is also plotted. It can be seen that the lower value of the error norm of ILMFM monotonically converges to the higher value of the error norm of LMFM, as a function of the number of integration points. The minimum value of the error is always obtained for only one integration point on each side of the local domain. This is a very important result that evidences that the ILMFM always leads to much better results than those obtained with the LMFM.

The discussion of this behavior takes into account a physical interpretation of results, as follows. The theorem of the total potential energy leads to an upper bound of the strain energy, which corresponds to a lower bound of the stiffness of the exact solution that actually settles in the body. Thus, the formulation of local numerical methods represents a lower bound of the strain energy which results in overestimating the stiffness of the system. Therefore, as Figure 17 shows, the solution of LMFM is always stiffer than the solution of ILMFM, obtained with one integration point, which is always very close to the exact solution of the problem. When additional segments, with one integration point, are considered in ILMFM, its solution monotonically converges to the solution of LMFM and hence, it can be concluded that the additional integration points monotonically increase the stiffness of ILMFM, obtained with only one integration point. The best solution is always obtained from the lower stiffness of ILMFM, obtained with only one integration point on each side of the local domain. This behavior is a common pattern of all numerical results of this paper. Note that the improvement of the solution accuracy, generated by the reduced integration, has

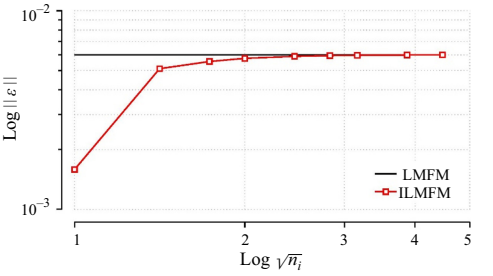

Figure 17.
Error norm in energy ε of ILMFM, as a function of the number of integration points n_i, equally spaced on each side of the local domain, for the discretization of $33 \times 5 = 165$ nodes

Note(s): LMFM, computed with 10 Gauss points on each side of the local domain, is also plotted for comparison. ILMFM monotonically converges to LMFM, as a function of the number of integration points, with the best result of ILMFM obtained for one integration point on each side of the local domain

been already used in the standard displacement assumed FEM, as a measure to prevent locking problems of fully integrated elements. As a final conclusion of this discussion, it is important to mention that the reduced integration, carried out by the linearly integrated local numerical methods presented in this paper, does not lead to any sort of spurious instability. This behavior is a direct consequence of having a total of four integration points, in the case of ILMFM, to compute the stiffness associated to each local node which, therefore, prevents the generation of spurious zero-energy modes, unlike nodal integration methods without stabilization. As a matter of fact, nodal integration in meshfree methods leads to instabilities due to the fact that each node is associated with a support domain, where shape function derivatives are integrated, to compute the nodal stiffness. This implies that each integration domain is associated with only one integration point, that is the node. Hence when only one integration point is considered for higher order functions, other than constant strain, the nodal integration causes instabilities.

7.6 Accuracy and convergence of ILMFM

Another test was performed to assess the solution accuracy and convergence of ILMFM. Three regular discretizations of the cantilever beam, with $65 \times 9 = 585$, $97 \times 13 = 1{,}261$ and $129 \times 17 = 2{,}193$ nodes were considered. ILMFM was applied with one integration point, on each side of the local domain, while LMFM was applied with 10 Gauss integration points, for comparison. Figure 18 presents the results for the solution accuracy and convergence rates obtained. As it can be clearly seen ILMFM, with one integration point on each side of the local domain, is always much more accurate than LMFM, with a stable convergence rate higher than the one of LMFM.

7.7 Condition number of ILMFM

When new numerical methods are developed, it is quite important to compute the condition number of the respective global stiffness matrix, an upper bound to the amplification of errors in structural properties and loads, to ensure the stiffness matrix is well conditioned. The

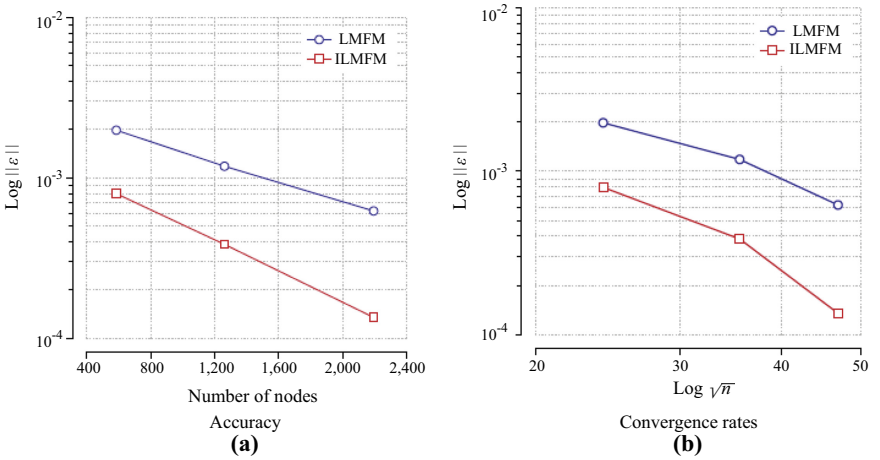

Figure 18. Accuracy and convergence rates, measured from the error norm in energy ε, for the cantilever-beam discretization with $65 \times 9 = 585$, $97 \times 13 = 1{,}261$ and $129 \times 17 = 2{,}193$ nodes n

Note(s): On each side of the local domain, ILMFM was applied with 1 integration point, on each side of the local domain, while LMFM used 10 Gauss integration points. ILMFM presents an excellent performance

analysis was carried out for both LMFM and ILMFM, as well as for the standard FEM, in order to compare the corresponding condition numbers. This comparison was performed using regular discretizations of the cantilever beam, with $33 \times 5 = 1{,}65$, $65 \times 9 = 585$ and $129 \times 17 = 2{,}193$ nodes, and a FEM mesh defined from the same nodal distribution by using bilinear quadrilateral finite elements, resulting in meshes with a total of $32 \times 4 = 128$, $64 \times 8 = 512$, $97 \times 13 = 1{,}261$ and $128 \times 16 = 2{,}048$ finite elements. Table 1 and Figure 19 present the results obtained in this analysis, where it can be seen that ILMFM always performs better than the other methods, with smaller values of the condition number, even outperforming the values of FEM for all nodal distributions. This is a clear evidence of the high level of numerical efficiency of ILMFM.

Another test was performed to analyze the influence of the number of integration points of ILMFM in the condition number of the global stiffness matrix. The analysis was carried out for ILMFM and LMFM for comparison, with the same nodal distribution of $129 \times 17 = 2{,}193$ nodes, used in the previous test. The results obtained, presented in Figure 19, show that the condition number of ILMFM is always lower than the corresponding number of LMFM; as the number of integration points increases, the condition number of ILMFM increases monotonically, from a minimum value that corresponds to a single integration point on each side of the local domain, until it eventually converges to an upper limit that corresponds to the value of the condition number of LMFM. This behavior, a natural consequence of the reduced integration performed by ILMFM, eventually ensures that the stiffness matrix of ILMFM, with 1 point on each side of the local domain, is always well conditioned.

7.8 Computational efficiency of ILMFM

The performance of ILMFM exhibits a clear reduction of the computational effort, when compared to other numerical methods, which is obviously a consequence of the formulation

Table 1. Condition number of the global stiffness matrix in local meshfree methods

Nodes	Condition number LMFM	FEM	ILMFM
165	1.05E+10	9.93E+09	8.09E+09
585	2.02E+10	1.58E+10	1.49E+10
2,193	2.83E+10	2.33E+10	2.01E+10

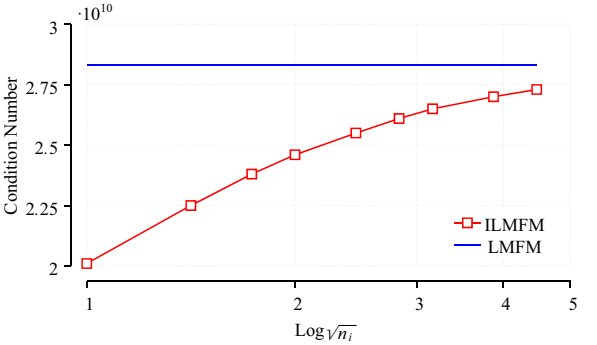

Figure 19. Results of the condition number of the global stiffness matrix

Note(s): Obtained by ILMFM, with a regular nodal discretization of the cantilever beam with 2,193 nodes, as a function of the number of integration points n_i; the condition number of LMFM is used for comparison

differences and implementation procedures. Hence, this section presents some evidence of this striking feature of ILMFM, through an assessment of the respective CPU time consumption. Following this objective, four regular discretizations of the cantilever-beam, with $33 \times 5 = 165$, $65 \times 9 = 585$, $97 \times 13 = 1{,}261$ and $129 \times 17 = 2{,}193$ nodes were considered. Only the major computational cost that is the cost of generating the global stiffness matrix and solving the system of algebraic equations was measured in this test. All the routines were compared when using MATLAB 2015a on an Intel Core I7-4700MQ computer with CPU of 2.4GHz and 16 GB of RAM. The test was carried out for ILMFM, LMFM, as well as for the EFG method, presented by Belytschko *et al.* (1994), the Meshless Local Petrov–Galerkin Finite Volume Method (MLPG-FVM), presented by Atluri *et al.* (2004) and the standard FEM, implemented through the routines presented by Kwon and Bang (2000). The FEM mesh was defined from the same nodal distributions by using bilinear quadrilateral finite elements, resulting in meshes with a total of $32 \times 4 = 128$, $64 \times 8 = 512$, $97 \times 13 = 1{,}261$ and $128 \times 16 = 2{,}048$ finite elements. To carry out the test, without compromising the accuracy, 10 Gauss integration points were used in LMFM, EFG and MLPG-FVM, four Gauss quadrature points were used in FEM, while one integration point, on each side of the local domain, was used in ILMFM. The results obtained, presented in Table 2 and Figure 20, show that the CPU time of ILMFM is always very much lower than the CPU time of LMFM, EFG and MLPG-FVM; the CPU time of ILMFM corresponds at the most, only to a small percentage of about 28% of the CPU time of MLPG-FVM, which can be computationally more efficient than FEM, as already reported by Moosavi and Khelil (2008); these very important results are also evident in Table 2 which shows that, for the discretization with 2,193 nodes, the CPU time of MLPG-FVM is about 55% of the CPU time

	CPU time (seconds)		
Nodes	EFG	LMFM	ILMFM
165	9.0220	6.07957	0.87022
585	60.7681	36.65571	4.47215
1,261	194.5159	97.67776	11.94385
2,193	338.2817	169.87100	20.77149
Nodes	MLPG-FVM	ILMFM	FEM
165	4.19016	0.87022	0.20228
585	16.06457	4.47215	3.15939
1,261	43.21458	11.94385	24.26805
2,193	75.15430	20.77149	134.88930

Table 2.
CPU time measured in local meshfree methods

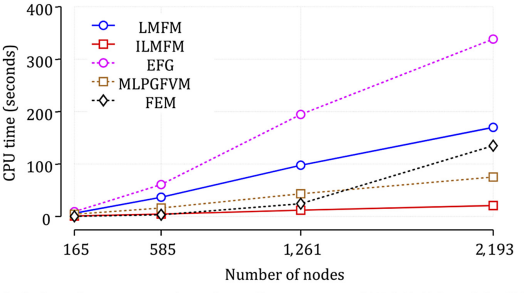

Note(s): The very high-level computational performance of ILMFM, with CPU time very much lower than the CPU time of FEM can be seen

Figure 20.
Results of the CPU time (s) obtained by ILMFM, LMFM, EFG, MLPG-FVM and FEM, with regular nodal distributions of the cantilever-beam discretization

of FEM, while ILMFM performs even better with CPU time of about only 15% of the respective value of FEM. Therefore, the conclusion that can be clearly drawn out of these tests is that the CPU time of ILMFM is very much lower than the CPU time of FEM. This is a remarkable result that undoubtedly evidences the very high level of the computational efficiency of ILMFM.

This assessment of the computational efficiency of ILMFM cannot be completed without showing that the low values of the CPU time, reported in Table 2, do not compromise the high level of accuracy of the method. This can be done through a comparison of ILMFM and MLPG-FVM results, against the exact solution. The MLPG-FVM was chosen due to its fast computing and excellent rate of convergence that even outperforms the FEM for some problems, see Atluri *et al.* (2004). Results were obtained for the same parameters and the same nodal distribution of $33 \times 5 = 165$ nodes of the cantilever-beam discretization.

As Figure 21 shows both methods present a high level of accuracy and a good agreement with the analytical solution, although ILMFM is definitively more accurate, under the same conditions. Therefore, the high level of the computational efficiency of ILMFM, associated with a remarkable accuracy, makes this a very reliable and robust meshfree numerical method.

7.9 Finite element discretization

To solve the benchmark problem, three regular discretizations of the cantilever beam, with $10 \times 4 \times 2 = 80$, $10 \times 6 \times 2 = 120$ and $10 \times 10 \times 2 = 200$ constant-strain triangular finite elements with corresponding 55, 77 and 121 nodes, were considered. Figure 22 represents an exploded view of the mesh with $10 \times 4 \times 2 = 80$ finite elements and 55 nodes.

The first test was carried out with the finite element mesh of 55 nodes, in order to make evident that both local finite element formulations, ILFEM and LFEM, generate identical global stiffness matrices which in turn are identical to the stiffness matrix generated by the standard FEM. Figure 23 shows images of these global stiffness matrices, where it can be easily seen that the matrices are effectively identical.

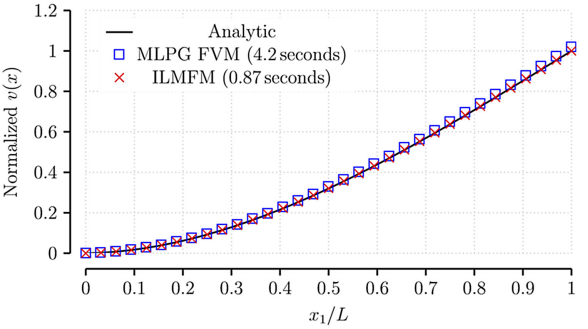

Note(s): Results show a good agreement with the analytical solution, although ILMFM is definitively more accurate

Figure 21.
Results of normalized vertical displacements for $x_1 = L/2$, obtained by ILMFM and MLPG-FVM, with a regular $33 \times 5 = 165$ nodal distribution of the cantilever-beam discretization

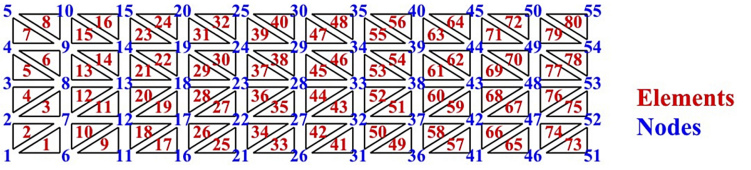

Figure 22.
An exploded view of the constant-strain finite-element mesh with $10 \times 4 \times 2 = 80$ elements and 55 nodes

Generating identical global stiffness matrices, for the same triangular finite element mesh discretization, implies that both the global and local formulations of the finite element method lead to the same solution accuracy which only depends on the discretization used. This statement becomes evident in Figure 24, which displays the displacement and energy error norms for ILFEM, LFEM and standard FEM, computed from the three meshes with corresponding 55, 77 and 121 nodes.

A final test aims assessing the computational efficiency of local formulations ILFEM and LFEM, against the standard FEM. The three finite element meshes with corresponding 55, 77 and 121 nodes were considered to perform this test. Only the cost of generating the global stiffness matrix and solving the system of algebraic equations was measured in this test. All

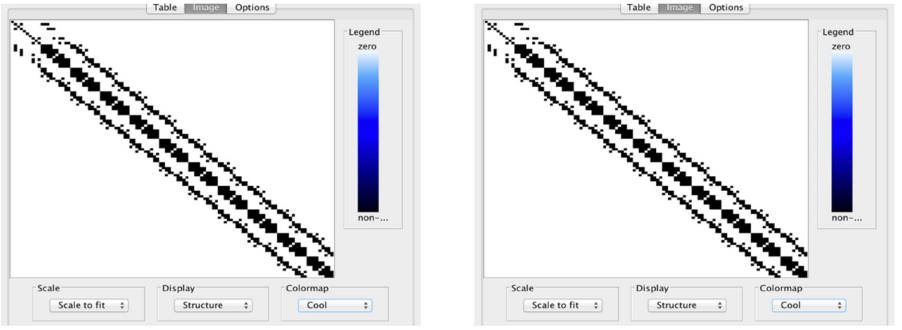

ILFEM and LFEM

(a)

Standard FEM

(b)

Note(s): It can be seen that ILFEM and LFEM generate a global stiffness matrix that is identical to the stiffness matrix generated by the standard FEM

Figure 23.
Images of the global stiffness matrix obtained for the finite element mesh with $10 \times 4 \times 2 = 80$ elements and 55 nodes

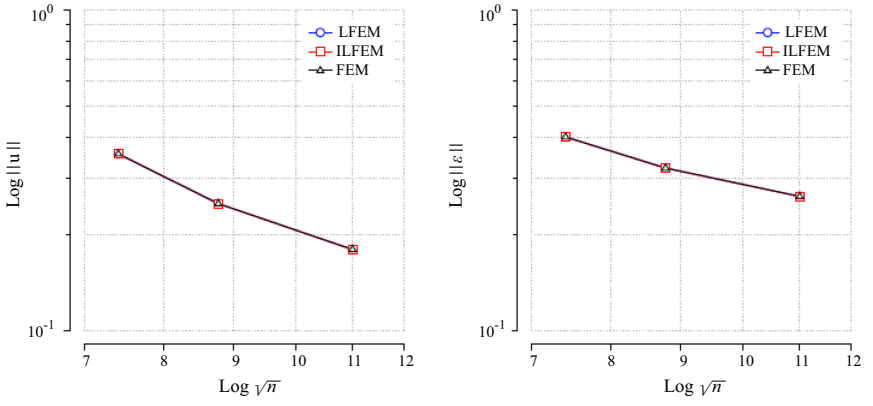

ILFEM and LFEM

(a)

Standard FEM

(b)

Note(s): Computed from the three constant strain finite element meshes with corresponding 55, 77 and 121 nodes,which are denoted by n. It can be seen that ILFEM, LFEM and standard FEM present the same solution accuracy

Figure 24.
Representation of displacement and energy error norms for ILFEM, LFEM and FEM

the routines were compared when using the CAS software Maple 2017, on a MacBook Pro computer, with processor 3,3 GHz Intel Core i7 and memory 16 GB 2133 MHz LPDDR3. The results obtained, presented in Table 3, show that the CPU time of the standard FEM is always lower than the CPU time of the local formulations ILFEM and LFEM, which is about three times the CPU time of the standard FEM. This is a consequence of the fact that local formulations generate the global stiffness matrix in a node-by-node stiffness calculation and, therefore, for each finite element of the mesh, the constant strain of the element is evaluated three times, in order to compute the element contribution for the corresponding nodal stiffness. This makes local formulations LFEM and ILFEM, less efficient than the standard FEM, where the stiffness of each finite element is computed only once, to be assembled in the global stiffness matrix of the body. This behavior, however, should be entirely different in a parallel processing environment, where local formulations are more appropriate, since they implement the node-by-node generation of the final system of equations.

8. Conclusions

New local formulations of meshfree and finite element numerical methods, in two-dimensional linear elastostatics, are presented in this paper.

The main feature of local numerical methods is the enforcement of a solution paradigm defined by a node-by-node calculation, to generate the rows of the global system of equations of a discretization of the body.

Kinematic formulations of the work theorem consider a particular convenient specification of the kinematically admissible strain field, leading thus to an equation of mechanical equilibrium, in the local domain, used to generate the respective stiffness matrix of the numerical method. A simple case of local equilibrium equations, based on a kinematically admissible strain field generated by a rigid-body displacement, is presented.

Two new meshfree numerical methods, LMFM and ILMFM, are presented in this paper. MLS approximation of the elastic field is used to implement both formulations, with rectangular local domains and quartic-spline MLS weight functions.

In LMFM, the local form of the equilibrium equation is a boundary integral, in the absence of body forces. Therefore, since the integration is carried out only on the boundary of the local domain, LMFM is computationally much more efficient than other meshfree methods that use domain integration with background cells.

On the other hand, in ILMFM, a linearly integrated local form of the equilibrium equation is discretely defined at the center point of each segment of the local domain. Consequently, ILMFM is computationally much more efficient than LMFM and other numerical methods that use standard numerical quadrature. In addition, the reduced integration of ILMFM, with only one point on each segment of the local domain, induces a reduction of the stiffness of the local node which consequently leads to an increase of the solution accuracy with no instabilities.

Three test problems were analyzed with ILMFM and LMFM, in order to assess the accuracy and efficiency of these formulations. The results obtained show that the use of the first-order monomial basis in MLS approximation is adequate; when the support size is kept

Table 3.
CPU time measured in local finite-element methods

Elements	CPU time (seconds) ILFEM	LFEM	FEM
80	0.663	0.665	0.284
120	0.956	0.959	0.369
200	1.605	1.609	0.551

small, more accurate and less-sensitive results are obtained. Effectively, a combination of first-order MLS, and a small support size, requires only a few neighboring nodes that lead to very fast computations.

All the numerical results obtained clearly demonstrate that ILMFM is an absolutely reliable and robust formulation. ILMFM and LMFM are locking-free methods, since they keep the respective typical convergence rate, when Poisson's ratio approaches the incompressible limit of $\nu = 0.5$; this is an evidence that there is no spurious stiffening in computations.

The linear integration of ILMFM, implemented with a single integration point on each segment of the local domain, led to remarkably accurate results with extremely fast computations. Numerical results obtained undoubtedly show that this method substantially reduces the computational effort necessary to build the stiffness matrix and therefore is computationally very efficient, when compared to other meshfree methods. Furthermore, since all the results obtained in the analysis are in perfect agreement with analytical solutions, the high level of accuracy and stability of the ILMFM implementation described herein make this a quite reliable and robust formulation of local kinematic meshfree methods.

Meshfree methods have been applied in almost all areas of structural and fracture mechanics; still, it is known that there are challenges in developing computationally efficient algorithms, with accurate integration techniques that can overcome the issue of the computational cost. The remarkable accuracy of the results with extremely fast computations makes it possible to apply ILMFM in the case of modeling nonlinear problems, where grid-based methods in general are not well suited. ILMFM can become an important tool in computational nonlinear solid mechanics, especially for solving problems with severe distortion, discontinuities and moving boundaries.

Two new local finite element methods, LFEM and ILFEM, are also presented in this paper. Local formulations of the finite element method use a new solution paradigm based in the node-by-node calculation to generate the rows of the global system of equations, while the global formulation uses the standard element-by-element stiffness calculation, that is assembled into the global stiffness matrix.

Local formulations associate to each node of the finite element mesh a global basis or shape function of compact support that gives a local character to the finite element approximation. Specifically, for each node of the finite element mesh, the compact support is defined around the respective node by the set of finite elements that share this node and, therefore, is coincident with the local domain of the respective node, where the equilibrium conditions resulting from the work theorem are defined.

The standard FEM has been commonly applied as a computer simulation method to solve a wide range of problems in a variety of practical fields, such as mechanical, aerospace, nuclear, chemical and civil engineering. Implementation of the finite element method in CAD systems on the basis of modern computers allows the solution of large-scale problems. Therefore, the introduction of parallel processing, a fast growing direction of research, is able to give the most significant result in terms of saving time designing and modeling. The finite element is the building block of the formulation procedure of the standard global formulation. On the other hand, local formulations of the finite element method, respectively LFEM and ILFEM, represent an efficient node based finite element method, especially on parallel processing, since they use a node-by-node algorithm for the finite element calculations. The final system of equations obtained through the node-by-node procedure, of the present local formulations, is equivalent to the one obtained through the element-by-element procedure of the standard FEM. However, in local formulations LFEM and ILFEM, the analysis processing can easily be parallelized, in terms of nodes, to set up and solve the global system of equations. Effectively, LFEM and ILFEM are quite suitable for parallel environments, because the respective algorithms based in a local domain coincident with the compact support, associated to each node, are spatially highly localized.

References

Atluri, S.N. and Shen, S. (2002), "The meshless local Petrov-Galerkin (MLPG) method: a simple and less-costly alternative to the finite element and boundary element methods", *CMES: Computer Modeling in Engineering and Sciences*, Vol. 3 No. 1, pp. 11-51.

Atluri, S.N. and Zhu, T. (1998), "A new Meshless Local Petrov-Galerkin (MLPG) approach in computational mechanics", *Computational Mechanics*, Vol. 22 No. 2, pp. 117-127.

Atluri, S.N. and Zhu, T. (2000), "New concepts in meshless methods", *International Journal for Numerical Methods in Engineering*, Vol. 47, pp. 537-556.

Atluri, S.N., Han, Z.D. and Rajendran, A.M. (2004), "A new implementation of the meshless finite Volume method through the MLPG mixed approach", *CMES: Computer Modeling in Engineering and Sciences*, Vol. 6, pp. 491-513.

Bathe, K.-J. (2014), *Finite Element Procedures*, Prentice Hall.

Beissel, S. and Belytschko, T. (1996), "Nodal integration of the element-free Galerkin method", *Computer Methods in Applied Mechanics and Engineering*, Vol. 139 Nos 1-4, pp. 49-74.

Belytschko, T. and Black, T. (1999), "Elastic crack growth in finite elements with minimal remeshing", *International Journal for Numerical Methods in Engineering*, Vol. 45, pp. 601-620.

Belytschko, T., Lu, Y.Y. and Gu, L. (1994), "Element-free Galerkin methods", *International Journal for Numerical Methods in Engineering*, Vol. 37, pp. 229-256.

Belytschko, T., Guo, Y., Liu, W.K. and Xiao, S. (2000), "A unified stability analysis of meshless particle methods", *International Journal for Numerical Methods in Engineering*, Vol. 48 No. 9, pp. 1359-1400.

Brebbia, C.A. (1985), "Variational basis of approximate models in continuum mechanics", in Brebbia, C.A. and Tottenham, H. (Eds), *Proc. of the II International Conference on Variational Methods in Engineering, Southampton, 1985*, Computational Mechanics Publications, Southampton and Springer Verlag, Berlin.

Chen, J.-S., Hillman, M. and Chi, S.-W. (2017), "Meshfree methods: progress made after 20 years", *Journal of Engineering Mechanics*, Vol. 143, p. 4.

Gingold, R.A. and Monaghan, J.J. (1977), "Smoothed particle hydrodynamics: theory and application to non-spherical stars", *Monthly Notices of the Royal Astronomical Society*, Vol. 181, pp. 375-389.

Hollister, S.J. and Kikuchi, N. (1994), "Homogenization theory and digital imaging: a basis for studying the mechanics and design principles of bone tissue", *Biotechnology and Bioengineering*, Vol. 43 No. 7, pp. 586-596.

Jamil, M. and Ng, E.Y.K. (2013), "Evaluation of meshless radial basis collocation method (RBCM) for heterogeneous conduction and simulation of temperature inside the biological tissues", *International Journal of Thermal Sciences*, Vol. 68, pp. 42-52.

Jin, C. and Suzuki, K. (2000), "Methodology and property of cover least square approximation", in *Transactions of the Japan Society for Computational Engineering and Science*, Vol. 2, pp. 213-218.

Kansa, E.J. (1990), "Multiquadrics: a scattered data approximation scheme with applications to computational fluid dynamics", *Computers and Mathematics with Applications*, Vol. 19 Nos 8-9, pp. 127-145.

Kirchhoff, G. (1859), "Uber das Gleichgewicht und die Bewegung einer unendlich diinnen elastischen Stabes", *Journal für die Reine und Angewandte Mathematik*, Vol. 56, pp. 285-313.

Kwon, Y.W. and Bang, H. (2000), *The Finite Element Method Using MATLAB*, 2nd ed., CRC Press.

Lee, S.H. and Yoon, Y.C. (2004), "Meshfree point collocation method for elasticity and crack problems", *International Journal for Numerical Methods in Engineering*, Vol. 61, pp. 22-48.

Libersky, L.D., Petscheck, A.G., Carney, T.C., Hipp, J.R. and Allahdadi, F.A. (1993), "High strain Lagrangian hydrodynamics", *Journal of Computational Physics*, Vol. 109, pp. 67-75.

Liu, G.R. and Gu, Y.T. (2001), "A local point interpolation method for stress analysis of two-dimensional solids", *Structural Engineering and Mechanics*, Vol. 11 No. 2, pp. 221-236.

Liu, G.R. and Yan, L. (2000), "A modified meshless local Petrov-Galerkin method for solid mechanics", *Proceedings of the Conference Advances in Computational Engineering and Sciences*, Los Angles, pp. 1374-1379.

Liu, W.K., Ong, J.S. and Uras, R.A. (1985), "Finite element stabilization matrices a unification approach", *Computer Methods in Applied Mechanics and Engineering*, Vol. 53, pp. 13-46.

Liu, W.K., Jun, S. and Zhang, Y.F. (1995), "Reproducing kernel particle methods", *International Journal for Numerical Methods in Engineering*, Vol. 20, pp. 1081-1106.

Liu, W.K., Chen, Y., Jun, S., Chen, J.S., Belytschko, T., Pan, C., Uras, R.A. and Chang, C.T. (1996), "Overview and applications of the reproducing kernel particle methods", *Archives of Computational Methods in Engineering State of the Art Reviews*, Vol. 3, pp. 3-80.

Liu, X., Liu, G.R., Kang, T. and Lam, K.Y. (2002a), "Radial basis point interpolation collocation method for 2D solid problem", in Liu, G.R. (Ed.), *Proceedings of the 1st Asian Workshop on Meshfree Methods*, World Scientific, pp. 35-40.

Liu, G.R., Yan, L., Wang, J.G. and Gu, Y.T. (2002b), "Point interpolation method based on local residual formulation using radial basis functions", *Structural Engineering and Mechanics*, Vol. 14, pp. 713-732.

Liu, G.R., Zhang, G.Y., Wang, Y.Y., Zhong, Z.H., Li, G.Y. and Han, X. (2007), "A nodal integration technique for meshfree radial point interpolation method (NI-RPIM)", *International Journal of Solids and Structures*, Vol. 44, Nos 11:12, pp. 3840-3860.

Lucy, L.B. (1977), "A numerical approach to the testing of the fission hypothesis", *Astronomical Journal*, Vol. 82 No. 12, pp. 1013-1024.

Melenk, J.M. (1995), "On generalized finite element methods", Ph.D. thesis, University of Maryland, College Park.

Melenk, J.M. and Babuska, I. (1996), "The partition of unity finite element method: basic theory and applications", *Computer Methods in Applied Mechanics and Engineering*, Vol. 139, pp. 289-314.

Moosavi, M.R. and Khelil, A. (2008), "Accuracy and computational efficiency of the finite Volume method combined with the meshless local Petrov-Galerkin in comparison with the finite element method in elasto-static problem", *ICCES: International Conference on Computational Engineering and Sciences*, Vol. 5, pp. 211-238.

Oliveira, T. and Portela, A. (2016), "Weak-form collocation – a local meshless method in linear elasticity", *Engineering Analysis with Boundary Elements*, Vol. 73, pp. 144-160.

Onate, E., Idelsohn, S., Zienkiewicz, O.Z. and Taylor, R.L. (1996), "A finite point method in computational mechanics: applications to convective transport and fluid flow", *International Journal for Numerical Methods in Engineering*, Vol. 39, pp. 3839-3867.

Portela, A. (1981), "Theoretical basis of boundary solutions for the linear theory of Structures", *J. Applied Mathematical Modelling*, Vol. 5 No. 1, pp. 57-59.

Shi, G.H. (1991), "Manifold method of material analysis", in *Transactions of the 9th Army Conference on Applied Mathematics and Computing*, Report No. 921, U.S. Army Research Office.

Strouboulis, T., Copps, K. and Babuska, I. (2000), "The generalized finite element method: an example of its implementation and illustration of its performance", *International Journal for Numerical Methods in Engineering*, Vol. 47 No. 8, pp. 1401-1417.

Truesdell, C. and Toupin, R. (1960), "Principles of classical mechanics and field theory", *Encyclopedia of Physics*, Vol. 2, Springer, Berlin.

Wu, Z. (1992), "Hermite-Birkhoff interpolation of scattered data by radial basis functions", *Journal of Approximation Theory*, Vol. 8, pp. 1-10.

Zhang, L. and Bathe, K.-J. (2017), "Overlapping finite elements for a new paradigm of solution", *Computers and Structures*, Vol. 187, pp. 64-76.

Zhang, X., Liu, X.H., Song, K.Z. and Lu, M.W. (2001), "Least-squares collocation meshless method", *International Journal for Numerical Methods in Engineering*, Vol. 51 No. 9, pp. 1089-1100.

Zienkiewicz, O.C. and Taylor, R.L. (1983), *Finite Element and Approximation*, John Wiley.

Further reading

Onate, E., Perazzo, F. and Miquel, J. (2001), "A finite point method for elasticity problems", *Computers and Structures*, Vol. 79, pp. 2151-2163.

Zhu, T., Zhang, J. and Atluri, S.N. (1998), "A local boundary integral equation (LBIE) method in computational mechanics and a meshless discretization approach", *Computational Mechanics*, Vol. 21, pp. 223-235.

Corresponding author

Artur Portela can be contacted at: aportela@unb.br